Asynchronous Machine with Wind Turbine IRFO Control

A. ALAZRAG, L. SBITA

University of Gabés, National engineering school of Gabés (ENIG),
Process laboratory, Energetic, Environment and Electrical system, TUNISIA

Abstract: The paper deals with a squirrel cage induction generator connected to the grid through a back-to-back converter driven by vector control. The stator-side converter controls the generator torque by means of an indirect vector control scheme. In order to reduce the system dependence from the mechanical system behavior, a torque loop is used in the current reference calculations. The battery energy storage system (BESS) plays a fundamental role in controlling and improving the efficiency of renewable energy sources. Stochasticity of wind speed and reliability of the main system components are considered. The grid-side converter controls the DC bus voltage and the reactive power in order to accomplish the grid codes. Speed control using flow directional control, indirect conventionally uses proportional integral (PI) type current regulators, which achieve satisfactory objectives on torque and flow dynamics. The objective of this article is to present an indirect vector control strategy with oriented rotor flux using current regulators of the proportional integral (PI) type, applied to an asynchronous machine supplied by a voltage inverter, capable of supplying during restrictive stresses, more satisfactory torque and flux responses. The obtained simulation results upon simulation tests of the global system are developed under the MATLAB / Simulink environment and are satisfactory .

Keywords: Renewable Energy,Wind Turbine, Asynchronous machine (SCIG),Battery storage ,Indirect Rotor flux orientation(IRFO),PI, electromagnetic torque, axis d,q.

Received: April 29, 2021. Revised: April 25, 2022. Accepted: May 29, 2022. Published: June 30, 2022.

1. Introduction

Energy has become a fundamental element because of our different demands in many domestic and industrial terms. This prompts us to always think about new techniques for producing this energy. Since the dawn of humanity, the production of energy has been based largely on fuels such as wood, fossils (coal, oil, gas…), then uranium. But the big problem accompanying the use of these materials is the emission of gases and the massive releases of various compounds; which unbalances our planet and pushes towards an open non-renewable cycle. In just over a century, energy with electricity as a modern form has taken a prominent place. Its production covers a third of the world's energy consumption which is concentrated mainly in thermo mechanical machines where combustion is on a large scale with the direct emission of several million tons of CO2 causing high degrees of pollution and temperature; as well as the reduction of nature reserves. So, we need to look for other alternatives to fossil fuels to produce electricity from renewable sources that are non-polluting and more economical by making good use of the elements of nature such as water, sun and wind. This is the goal of our study, which focuses on one of the renewable energies in development at the time, which is wind energy. The reliable and cost-effective wind turbine is the ideal source of electricity for many applications. Wind turbines come in many sizes, from small wind turbines of a few watts to megawatt wind turbines feeding the electricity grid. The largely dominant technology today is horizontal axis, three-bladed and sometimes two-bladed windward rotor turbines. These wind turbines have a nominal power between 5KW and 5MW, they can operate at fixed speed or at variable speed [12][13]. The types of generators associated with wind turbines are asynchronous machines and synchronous machines in their different variants. Among all the renewable energies contributing to the production of electricity, wind energy currently holds the star of renewable for regions and countries with enormous wind potential. It is one of the most promising, in terms of ecology, competitiveness, scope and creation of jobs and wealth. We will focus on the technological advances that have allowed the construction and proper functioning of wind turbines and their integration into electricity production. In order to better exploit wind resources for different wind conditions, this study focuses on the Asynchronous Machine with indirect orientation of the rotor flux which is the heart of a large part of current wind turbines due to its advantages relative to other electromagnetic actuators. Dynamic management of interconnected grid-connected wind farm storage systems would therefore be necessary to ensure the mitigation of variable wind farm output variability and to maintain grid power stability [29]. Based on the state of charge (SOC) of the BESS authors proposed an algorithm for dynamic programming in order to smoothly fluctuate wind power [30]. Different application of strategies have been applied for wind farm active power control, voltage control. SCIG

control can be implemented using different approaches : scalar or vector control, direct or indirect field orientation, rotor or stator field orientation [12][13]. Scalar control [15] is simple to implement, but easily unstable. A better performance is obtained with direct vector control, requiring sensed flux values to define and control the field orientation references. This, however means that it is necessary to use hall-effect sensors, which, inpractise, is problematic, and expensive,[14][16]. The indirect field-orientation method is more sensitive to the machine parameters but removes the necessity of direct flux sensing[15][16]. This paper proposes an indirect vector control strategy less sensitive from the machine parameters than the conventional scheme[8]. The wind turbines are also equipped with a control system based on electronic converters to adapt to wind conditions. This work is organized as follows: The Section II presents a modeling of the wind turbine connected to the grid as well as a modeling in a two-phase reference frame (the adapted model is based on the Park transformation) linked to the rotating field with a view to supply and control by static converters. of the double feed asynchronous machine. The Section III,study of storage system. The Section V implements the indirect vector control of the squirrel cage asynchronous generator based on a PI (Proportional Integral) regulator, Section IV the control ensures the decoupling of the d and q axes, the purpose of which is to improve the behavior static and dynamic system. The Section VII, is reserved for simulation results with interpretation of these results.

2. Modeling of a wind turbine with induction generator

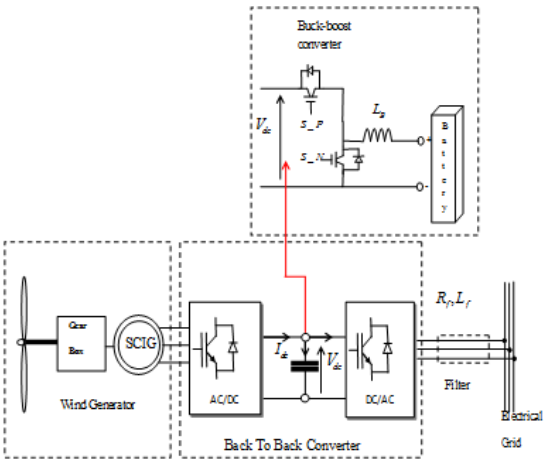

Figure 1: Wind turbine with SCIG connected to electrical grid

The system being analyzed can be seen in Figure 1. It is important to point out that there are more elements, e.g. a transformer and a wind farm grid, which are not included in the present paper. The squirrel cage induction generator (SCIG) is attached to the wind turbine by means of a gearbox. The SCIG stator windings are connected to a back to back full power converter.

2.1 Wind turbine

A wind energy conversion system (WECS) transforms wind kinetic energy to mechanical energy by using rotor blades. This energy is then transformed into electric energy by a generator, so the turbine is one of the most important elements in wind turbine. In order to better understand the process of wind energy conversion, descriptions of the major parts of a wind turbine are given in this section. According to Newton's law, the kinetic energy for the wind with particular wind speed is described as:

$$E_m = \frac{1}{2} m.V_v^2 \tag{II.1}$$

Where m represents the mass of the wind, and its power can be written as :

$$P_m = \frac{1}{2}.C_p(\lambda,\beta).\rho.S.V_v^3 \tag{II.2}$$

Where : S : Blade swept area (m^2), ρ : Specific density of air(Kg/m^3)

V_v : wind speed (m/s), $C_p(\lambda,\beta)$: Power coefficient, λ : speed ratio, β : pitch angle With :

$$\lambda = \frac{R.\Omega}{V_v} \tag{II.3}$$

Ω :Mechanical turbine speed (rad/s), R : radius of the turbine blade (m).
We can derive the formula of the torque which is :

$$T_t = \frac{1}{2.\Omega_t}.C_p(\lambda,\beta).\rho.\pi.R^2.v^3 \tag{II.4}$$

Where $\mathbb{C}_p$is the power coefficient of the turbine which is obtained from the following equation :

$$C_p(\lambda,\beta) = K_1.(\frac{K_2}{\lambda} - K_3.\beta - K_4)e^{\frac{K_5}{\lambda}} + K_6.\lambda \tag{II.5}$$

With :

$$\frac{1}{\lambda} = \frac{1}{(\lambda + 0.08.\beta)} - \frac{0.035}{\beta^3 + 1} \tag{II.6}$$

Where : $k_1 = 0.5176, k_2 = 116, k_3 = 0.4, k_4 = 5, k_5 = 21 \text{and} k_6 = 0.006$
This Figure shows the evolution of the power coefficient as a function of λ for different values of β. The maximum is obtained for an optimum pitch angle β_{opt}=0 and a relative speed λ_{opt}=0 .

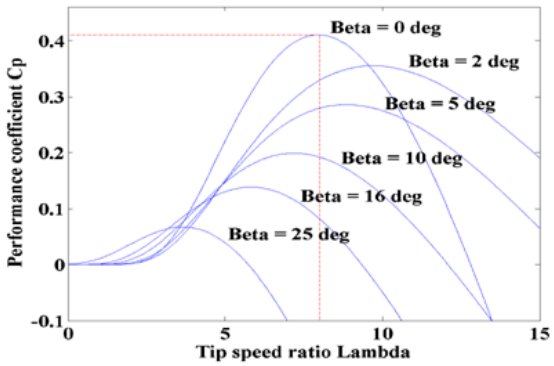

Figure 2: Evolution of the power coefficient according to λ and β

With the dependence on the λ and β, maximum value of Cp could be reached and maintained through controlling the pitch angle and generator speed at particular wind speed. A group of typical Cp – λ curves for different β is shown in Figure 2 and there is always a maximum value for Cp at one particular wind speed. It is found that the power coefficient is a function of λ and β, and in order to reach the maximum energy extracted from the wind turbine. The following equations show the values to be considered:

$$T_{opt} = \frac{1}{2}.\frac{C_{p\max}(\lambda).\rho.S.R^3}{\lambda_{opt}^3}.\Omega^2 \quad \text{(II.7)}$$

$$\Omega_{ref} = \frac{\lambda_{opt}}{R}.V_v \quad \text{(II.8)}$$

2.1.1 Gearbox

The gear box provides speed and torque conversions from a rotating power source to another device, using gear ratios. A gearbox is often used in a wind turbine to increase the rotational speed from a low-speed main shaft to a high-speed shaft connecting with an electrical generator. A gear box is mathematically modeled by the following equations:

$$\begin{cases} \Omega_g = K_g.\Omega_T \\ T_g = \frac{1}{K_g}.T_T \end{cases} \quad \text{(II.9)}$$

With : K_g is the speed gear box gain $K_g \leq 0$ For our study, we chose a wind turbine with direct coupling

2.1.2 Driveshaft dynamic equation

The differential equation which makes it possible to determine the evolution of the mechanical speed from the total mechanical torque (t_m) is given by:

$$J.\frac{d\Omega_m}{dt} = T_m \quad \text{(II.10)}$$

Where: J is the total inertia brought back to the generator shaft, including the inertia of the turbine, the gearbox and the generator. The mechanical torque deduced from this coupling is the sum of all the torques applied to the rotor:

$$T_m = T_g - T_{em} - f\Omega_g \quad \text{(II.11)}$$

With:
T_m: is Electromagnetic torque developed by the generator,
T_g : gear box torque,
f: Total coefficient of friction of the mechanical coupling.

2.2 Asynchronous machine (SCIG)

The conversion of mechanical energy to electric energy is performed by the turbine and the generator. Different generator types have been used in wind energy systems. These include the squirrel cage induction generator (SCIG), doubly fed induction generator (DFIG), and synchronous generator (SG) [1]. The SCIG is simple and rugged in construction. It is relatively inexpensive and requires minimum maintenance. The SCIGs are also employed in variable-speed wind energy systems. To date, the largest SCIG wind energy systems are around 4 MW in offshore wind farms. The voltage equations for the stator and rotor of the generator in the reference of Park with two axes (d,q), [3], [5].

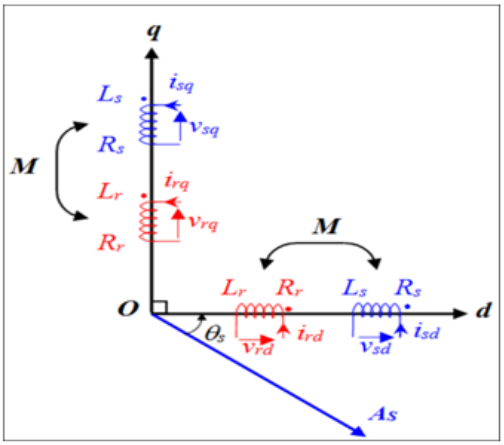

Figure 3: Representation of fictitious windings of d-q axes

For the machine equations, assuming that the stator and rotor windings are sinusoidal and symmetrical [14],[16], the relation between voltage and currents on a synchronous reference dq can be written as:

$$\begin{bmatrix} v_{sd} \\ v_{sq} \end{bmatrix} = \begin{bmatrix} R_s 0 \\ 0 R_s \end{bmatrix} \begin{bmatrix} i_{sd} \\ i_{sq} \end{bmatrix} + \frac{d}{dt} \begin{bmatrix} \phi_{sd} \\ \phi_{sq} \end{bmatrix} + \begin{bmatrix} 0 & -\omega_s \\ \omega_s & 0 \end{bmatrix} \begin{bmatrix} \phi_{sd} \\ \phi_{sq} \end{bmatrix} \quad \text{(II.12)}$$

$$\begin{bmatrix} 0 \\ 0 \end{bmatrix} = \begin{bmatrix} R_r 0 \\ 0 R_r \end{bmatrix} \begin{bmatrix} i_{rd} \\ i_{rq} \end{bmatrix} + \frac{d}{dt} \begin{bmatrix} \phi_{rd} \\ \phi_{rq} \end{bmatrix} + \begin{bmatrix} 0 & -\omega_r \\ \omega_r & 0 \end{bmatrix} \begin{bmatrix} \phi_{rd} \\ \phi_{rq} \end{bmatrix} \quad \text{(II.13)}$$

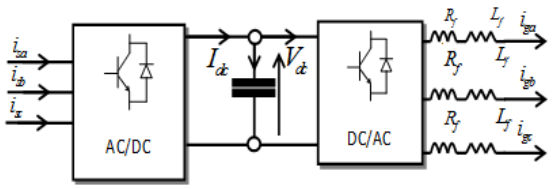

Figure 4: Back to Back converter

$$\begin{bmatrix} \phi_{sd} \\ \phi_{sq} \end{bmatrix} = \begin{bmatrix} L_s \mathrm{M} \\ ML_r \end{bmatrix} \begin{bmatrix} i_{sd} \\ i_{sq} \end{bmatrix} \quad \text{(II.14)}$$

And

$$\begin{bmatrix} \phi_{rd} \\ \phi_{rq} \end{bmatrix} = \begin{bmatrix} L_s \mathrm{M} \\ ML_r \end{bmatrix} \begin{bmatrix} i_{rd} \\ i_{rq} \end{bmatrix} \quad \text{(II.15)}$$

With : V_s: Stator voltage, (i_s, i_r) : stator and rotor current,(phi_s, phi_r) : stator and rotor flux, $(\mathbb{R}_s, \mathbb{R}_r)$:stator and rotor resistance, (L_s, L_r):stator and rotor inductance , M : mutual inductance , d : d-axis, q : q-axis. We become to replace the flux with their expressions according to the currents; in using (10) and (11), the model of the three-phase asynchronous machine in the axis coordinate system (d,q) will be given in matrix form :

$$\begin{bmatrix} v_{sd} \\ v_{sq} \\ 0 \\ 0 \end{bmatrix} = \begin{bmatrix} R_s + L_s(d/dt) & -L_s\omega_s M(d/dt) & -\mathrm{M}\omega_s \\ L_s\omega_s R_s + L_s(d/dt)\mathrm{M}\omega_s M(d/dt) & & \\ M(d/dt) & -M\omega_r R_r + L_r(d/dt) & -L_r\omega_r \\ M\omega_r M(d/dt) & L_r\omega_r R_r + L_r(d/dt) & \end{bmatrix} \begin{bmatrix} i_{sd} \\ i_{sq} \\ i_{rd} \\ i_{rq} \end{bmatrix} \quad \text{(II.16)}$$

This leads to the equivalent diagram coupled with an asynchronous machine along axis d.

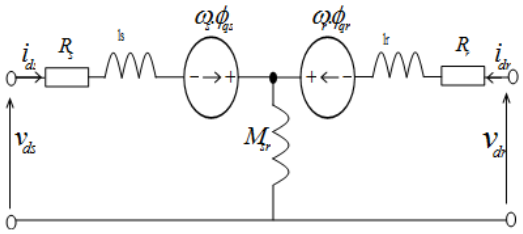

Figure 5: Equivalent diagrams coupled of an asynchronous machine according to the axis d

Also, the equivalent diagram coupled of an asynchronous machine according to the axis q.

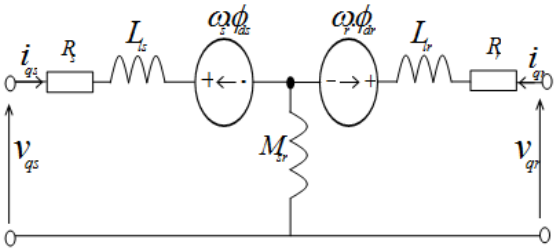

Figure 6: Equivalent diagrams coupled of an asynchronous machine according to the axis q

With : $ls = L_s - M, \quad lr = L_r - M$ Expression of electromagnetic torque In the general case, the instantaneous electrical power Pe supplied to the windings stator and rotor is expressed as a function of the axis sizes d, q:

$$P_e = v_{sd}.i_{sd} + v_{sq}.i_{sq} \quad \text{(II.17)}$$

It breaks down into three series of terms: *.Power dissipated in Joule losses:

$$R_s(i_{sd}^2 + i_{sq}^2) + R_r(i_{rd}^2 + i_{rq}^2) \quad \text{(II.18)}$$

**. Power transmitted to the rotor in the form of a variation of magnetic energy :

$$i_{sd}(d\phi_{sd}/dt) + i_{sq}(d\phi_{sq}/dt) + i_{rd}(d\phi_{rd}/dt) + i_{rq}(d\phi_{rq}/dt) \quad \text{(II.19)}$$

***. Mechanicanical power

$$P_m = (i_{sq}.\phi_{sd} - i_{sd}\phi_{sq})\omega_s + (i_{rq}\phi_{rd} i_{rd}\phi_{rq})\omega_r \quad \text{(II.20)}$$

The electromagnetic torque developed by the machine is given by the expression:

$$C_{em} = \frac{P_m}{\Omega} \text{and} \Omega = \frac{\omega}{p} \quad \text{(II.21)}$$

Then the scalar expression of torque :

$$C_{em} = p.(\phi_{sd} i_{sq} - \phi_{sq} i_{sd}) \quad \text{(II.22)}$$

It is possible to obtain other expressions of the instantaneous torque by using the stator flux expressions:

$$C_{em} = p.\frac{M}{L_r}.(\phi_{rd} i_{sq} - \phi_{rq} i_{sd}) \quad \text{(II.23)}$$

Also :

$$C_{em} = p.M.(i_{rd} i_{sq} - i_{rq} i_{sd}) \quad \text{(II.24)}$$

This very important relationship highlights the fact that the torque results from the interaction of components of quadrature stator and rotor currents[9],[10]. The active and reactive power yields :

$$P = \frac{3}{2}.(v_{sd} i_{sd} + v_{sq} i_{sq}) \quad \text{(II.25)}$$

And :

$$Q = \frac{3}{2}.(v_{sq} i_{sd} - v_{sd} i_{sq}) \quad \text{(II.26)}$$

Active and reactive power, provided by the grid-side converter, can be expressed as:

$$P_g = \frac{3}{2}.(v_{gd}i_{gd} + v_{gq}i_{gq}) \quad \text{(II.27)}$$

/

$$Q_g = \frac{3}{2}.(v_{gq}i_{gd} - v_{gd}i_{gq}) \quad \text{(II.28)}$$

3. Battery storage

For the proper functioning of the hybrid energy system, the storage system plays a crucial role, it allows for continuity of service and better quality of energy supplied. We recall some electrical parameters used to characterize a battery, these are:

• Nominal capacitor (Qn): This is the maximum number of ampere-hours (Ah) that can be extracted from the battery, for given discharge conditions.

• The state of charge "SOC" (State Of Charge): This is the ratio between the capacity at time q(t) and the nominal capacity Qn, is :

$$SOC(t) = \frac{q(t)}{Q_n}, \text{with}(0 \leq \text{SOC} \leq 1) \quad \text{(III.1)}$$

If SOC=1 the battery is totally charged and if SOC=0 the battery is totally discharged.

• The charging cycle (or discharging): This is the parameter which reflects the relationship between the nominal capacity of a battery and the current at which it is charged (or discharged). It is expressed in hours.

•Cycle life : This is the number of charge/discharge cycles that the battery can sustain before losing 20% of its nominal capacity[5].

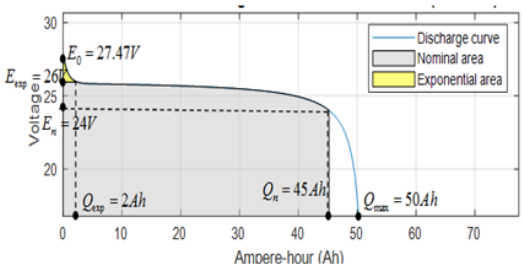

Figure 7: Battery discharge curve

By analyzing the figure above, we can see the presence of three specific points on the characteristic (Q-V): these three points are: the full load voltage (E0), the voltage corresponding to the end of the exponential zone (Eexp) and the corresponding voltage at the end of the nominal zone (En). The charge and discharge equations are given as follows [7]:

*Discharge :

$$E_B = E_0 - Ri - K\frac{Q}{Q - i_t}(i_t + i^*) + E_{\exp}(t) \quad \text{(III.2)}$$

//

*Charge :

$$E_B = E_0 - Ri - K\frac{Q}{Q - i_t}i^* - K\frac{Q}{Q - i_t}i_t + E_{\exp}(t) \quad \text{(III.3)}$$

With : $E_{\exp}(t) = B.|i(t)|.(-E_{\exp}(t) + A.sel(t))$ Figure 8 shows the discharge characteristic of the storage system used and the evolution of its voltage for different discharge currents.

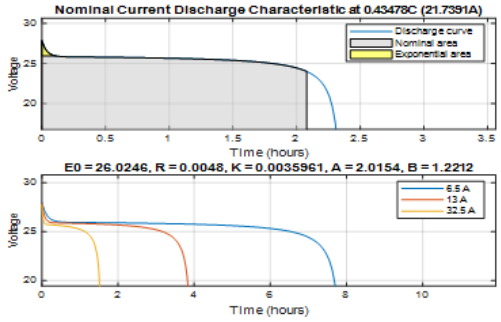

Figure 8: Characteristic VB = f(t) for different discharge currents.

The bidirectional DC DC converter is a combination of boost and buck converters. Such a converter is used to charge and discharge the battery.

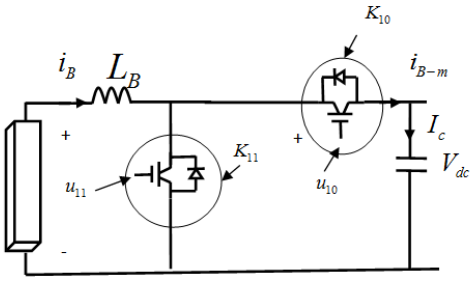

Figure 9: Circuit of the DC–DC bidirectional converter

3.1 Boost Mode

The boost mode is applied for the discharging procedure of the battery storage. Figure shows the circuit of the boost mode operation of the converter, where the direction of the inductor current is from the lower voltage side to the higherK1 voltage side . The averaged large signal inductor current, $\imath_L$, and the DC-bus output voltage, V_dc , in a continuous conduction mode (CCM) of operation can be found using the equations below. is closed ($K_1$0=1) and is open ($K_1$1=0).

$$L\frac{di_B}{dt} = V_B - V_{dc} \quad \text{(III.4)}$$

3.2 Buck Mode Operation

The buck mode is applied for the charging process of the battery storage. Figure present the circuit of the buck mode operation converter. In contrast to the buck mode operation, the inductor current flows from the higher voltage side to the lower voltage side . The averaged large signal inductor current, $\imath_L$, and the output battery voltage, V_B , are calculated by the equations below, and describe the buck-mode operation in a CCM of the converter. is open ($K_1$0=0) and is closed ($K_1$1=1)

$$L\frac{di_B}{dt} = V_B \tag{III.5}$$

By analyzing these two configurations, we can conclude that the relationships between the input quantities (V_B, i_B) and the output quantities (V_dc, i_{B-m}) of the converter are given by the system of equations below

$$\begin{cases} L\frac{di_B}{dt} = V_B - V_{dc}(1-u_{11}) \\ i_{B-m} = I_B(1-u_{11}) \end{cases} \tag{III.6}$$

4. Inverter modeling

The three-phase voltage inverter allows the exchange of energy between a DC voltage source and a three-phase inductive load [2].

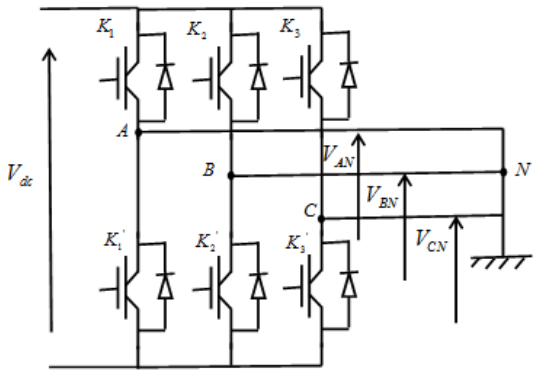

Figure 10: Simplified model of the DC/AC converter

The three-phase system is considered balanced so we can write:

$$V_a + V_b + V_c = 0 \tag{IV.1}$$

The corresponding PWM gate signals for the converter. To a 2 level three-phase voltage source inverter, there are six switches of three legs in inverter controlling the phase voltage and thus the current of induction generator. By defining the ON and OFF states of upper switch by 1 and 0, respectively, for one leg, there exist up to eight different states for inverter outputs. They are summarized in table 1 as well as the resulted phase voltage in ABC and $\alpha\beta$ frames. Eight inverter output voltages can be considered as eight voltage vectors [0, 0, 0] through [1, 1, 1].

Table 1: the phase-to-phase and phase to phase voltages of the inverter according to the states of the switches

S_C	S_B	S_A	V_C	V_B	V_A	U_{CA}	U_{BC}	U_{AB}
0	0	0	0	0	0	0	0	0
0	0	1	$-V_{dc}/3$	$-V_{dc}/3$	$2V_{dc}/3$	$-V_{dc}$	0	V_{dc}
0	1	0	$-V_{dc}/3$	$2V_{dc}/3$	$-V_{dc}/3$	0	V_{dc}	$-V_{dc}$
0	1	1	$-2V_{dc}/3$	$V_{dc}/3$	$V_{dc}/3$	$-V_{dc}$	V_{dc}	0
1	0	0	$2V_{dc}/3$	$-V_{dc}/3$	$-V_{dc}/3$	V_{dc}	$-V_{dc}$	0
1	0	1	$V_{dc}/3$	$-2V_{dc}/3$	$V_{dc}/3$	0	$-V_{dc}$	V_{dc}
1	1	0	$V_{dc}/3$	$V_{dc}/3$	$-2V_{dc}/3$	V_{dc}	0	$-V_{dc}$
1	1	1	0	0	0	0	0	0

The composed voltages delivered by the two level three phase inverter as a function of the state of the IGBTs are given by the following equations:

$$\begin{cases} U_{AB} = V_{dc}(S_A - S_B) \\ U_{BC} = V_{dc}(S_B - S_C) \\ U_{CA} = V_{dc}(S_C - S_A) \end{cases} \tag{IV.2}$$

Knowing that composed voltages are expressed as a function of phase-to-neutral voltages by the following equations:

$$\begin{cases} U_{AB} = V_A - V_B \\ U_{BC} = V_B - V_C \\ U_{CA} = V_C - V_A \end{cases} \tag{IV.3}$$

Then :

$$\begin{cases} V_A = \frac{V_{dc}}{3} * (2 * S_A - (S_B + S_C)) \\ V_B = \frac{V_{dc}}{3} * (2 * S_B - (S_A + S_C)) \\ V_C = \frac{V_{dc}}{3} * (2 * S_C - (S_B + S_A)) \end{cases} \tag{IV.4}$$

4.1 Filter technology

The integrated filter is of the low pass type, its purpose is to improve the quality of the signals exchanged between the converter and the grid parameter connection (R_f, L_f). Its cut frequency (f_c) is given by relation below:

$$f_c = \frac{R_f}{2.\pi.L_f} \tag{IV.5}$$

Par application de la transformée de Laplace, les courants à la sortie du filtre $(\mathbb{R}_f, Ł_f)$ seront alors exprimés comme suit:

$$\begin{cases} I_{dgrid} = \frac{V_{dcr} - V_{dgrid} + \omega.L_f.I_{qgrid}}{R_f + p.L_f} \\ I_{qgrid} = \frac{V_{qcr} - V_{qgrid} - \omega.L_f.I_{dgrid}}{R_f + p.L_f} \end{cases} \tag{IV.6}$$

Numerically , we write :

$$\begin{cases} I_{dcr}(n) = \frac{1}{2.\pi.f_c.T_e + 1}.I_{dcr}(n-1) + \frac{1}{L_f}.\frac{V_{dcr}(n) + \omega.L_f.I_{qcr}(n) - V_{dgrid}(n)}{2.\pi.f_c + \frac{1}{T_e}} \\ I_{qcr}(n) = \frac{1}{2.\pi.f_c.T_e + 1}.I_{qcr}(n-1) + \frac{1}{L_f}.\frac{V_{qcr}(n) - \omega.L_f.I_{dcr}(n) - V_{qgrid}(n)}{2.\pi.f_c + \frac{1}{T_e}} \end{cases} \tag{IV.7}$$

Where Te is the sampling period.

5. Oriented rotor flux control

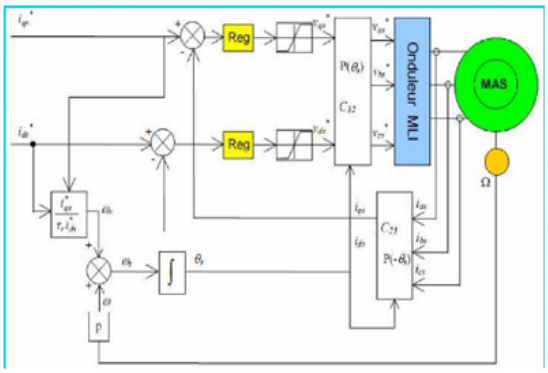

Figure 11: General diagram of the oriented rotor flux vector control

The control vector orientation of the rotor flux is the most used, because it eliminates the influence of the rotor and stator leakage reactance and gives better results than the methods based on the orientation of the stator flux or air gap [1], [3], while ensuring the best torque behavior as a function of the slip speed in steady state. According to the general vector control scheme with oriented rotor flux is as follows: The command is carried out by orienting the rotor flux along the direct axis "d" of the rotating frame is :

I_{sd}:it is the excitation current generates and controls the excitation flux ϕ_r .
I_{sq}: it is the armature current, which at a given excitation flux controls the torque. We impose that : $\Phi_{rd} = \Phi_r et \Phi_{rq} = 0$ then :

$$C_e = p\frac{L_m}{L_r}\Phi_r i_{sq} \qquad \text{(V.1)}$$

These expressions show that the flux depends only on the direct component of the stator current ids, and that if the latter is kept constant, the torque will only depend on the quadrature component of the stator current iqs. However, in the case of a voltage supply vsd and vsq influence both ids and iqs, therefore on the flux and the torque, hence the interest of adding compensation terms in order to make the axes d and q completely independent.

5.1 Indirect rotor flux orientation

The principle of this method consists in not using the magnitude of the rotor flux but simply its position calculated with reference sizes. In this method we do not need a sensor, an estimator or an observer of flux [13], [15], [16], [17]. therefore we have no knowledge of the modulus and phase of the rotor flux, this requires a measurement of the position of the rotor. Figure represents the block diagram of an indirect vector control with oriented rotor flux of an asynchronous machine.

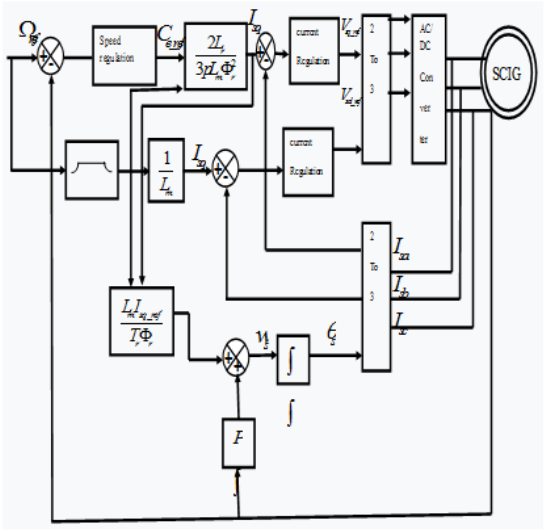

Figure 12: Block diagram of indirect rotor

6. Grid side converter

6.1 Control strategy

The equation of a MAS used to define the transfer functions required for the synthesis of regulators of speed and stator currents. The different regulators used in the regulation loops will be of the type proportional and integral (PI), because the quantities to be regulated are continuous quantities. We therefore have 3 regulators diagram :

6.1.1 The speed regulator

: It takes the reference speed and the measured speed as input. It acts on the torque (that is to say its output is the reference torque) to regulate the speed.

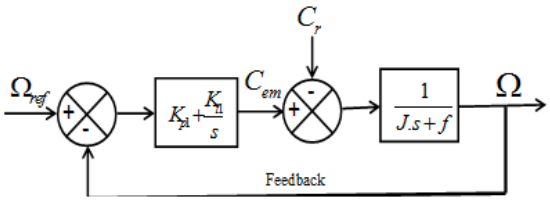

Figure 13: functional diagram of speed control

$$\frac{\Omega(s)}{\Omega_{ref}(s)} = \frac{(\frac{1}{J.s+f})(K_{p1}+\frac{K_{i1}}{s})}{1+(\frac{1}{J.s+f})(K_{p1}+\frac{K_{i1}}{s})} = \frac{1+\tau_1.s}{1+(\tau_1+\frac{f}{K_{i1}}).s+\frac{J}{K_{i1}}.s^2} \qquad \text{(VI.1)}$$

With : $\tau_1 = \frac{K_{p1}}{K_{i1}}$ This transfer function has a 2nd order dynamic. Denominator in the canonical form, we have to

solve the following system of equations:

$$\begin{cases} \frac{J}{K_{i1}} = \frac{1}{\omega_0^2} \\ \frac{2\xi}{\omega_0} = \tau_1 + \frac{f}{K_{i1}} \end{cases} \quad \text{(VI.2)}$$

For critical damping $\xi = 1$, we obtained :

$$\begin{cases} K_{p1} = \tau_1 . K_{i1} \\ K_{i1} = \frac{4.J}{\tau_1^2} \end{cases} \quad \text{(VI.3)}$$

6.1.2 The current regulator

: To ensure that the actual currents follow the set point currents, regulators currents acting on the control voltages are essential, we are interested in the sizing of regulators. So the two regulators are identical. The current regulation loop respectively Isd and Isq can be represented by the figure :

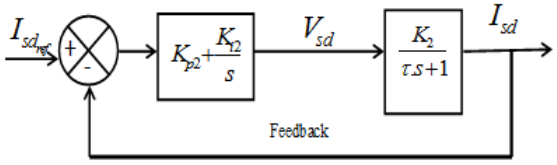

Figure 14: functional diagram of Isd current regulation

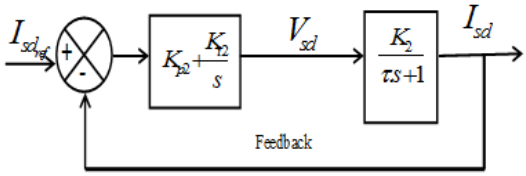

Figure 15: functional diagram of Isq current regulation

With :

$$K_2 = \frac{1}{R_s + (\frac{L_m}{L_r})^2 . R_r} \quad \text{(VI.4)}$$

$$\tau = \frac{\sigma . L}{R_s + (\frac{L_m}{L_r})^2 . R_r} \quad \text{(VI.5)}$$

The closed loop transfer function will therefore be :

$$\frac{I_{sd}(s)}{I_{sd_{ref}}(s)} = \frac{(\frac{1}{1+\tau.s})(K_{p2} + \frac{K_{i2}}{s})}{1 + (\frac{1}{1+\tau.s})(K_{p2} + \frac{K_{i2}}{s})} = \frac{(\frac{K_{p2}.K_2}{\tau}).s + \frac{K_{i2}.K_2}{\tau}}{s^2 + (\frac{K_{p2}.K_2+1}{\tau}) + \frac{K_{i2}.K_2}{\tau}} \quad \text{(VI.6)}$$

The characteristic closed loop equation looks like this:

$$s^2 + 2\xi\omega_0 s + \omega^2 = 0 \quad \text{(VI.7)}$$

For identification :

$$\begin{cases} K_{p2} = \frac{2\xi\omega_0\tau - 1}{K_2} \\ K_{i2} = \frac{\omega_0^2}{K_2} \end{cases} \quad \text{(VI.8)}$$

6.2 Grid-side converter

The control of the electrical system of the grid is configured in order to control the DC bus voltage and the reactive power which is consumed or supplied by the converter of the grid side. The DC bus voltage reference and the grid voltage level are used to determine the current references which determine the voltages to be applied on the grid side. figure 16 depicts the block diagram of grid side control.

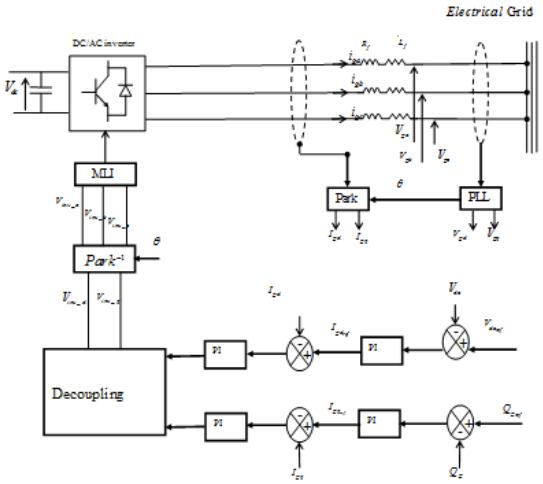

Figure 16: Block diagram of grid side converter control

To adjust the voltage Vdc, we can act on the active power Pg, and its reference value is obtained by the reference value of the power ¶$_{dc}$ which is given by:

$$P_{dc_{ref}} = V_{dc} . I_{dc_{ref}} \quad \text{(VI.9)}$$

By applying the Laplace transformation , we obtain:

$$\frac{V_{dc}}{I_{dc}} = \frac{1}{C.s} \quad \text{(VI.10)}$$

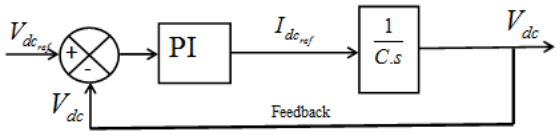

Figure 17: functional diagram of DC bus voltage

6.3 Phase locked loop

The PLL is used to provide a unity power factor operation which involves synchronization of the inverter output current with the grid voltage and to give a clean sinusoidal current reference [14]. The PI controller parameters of the PLL structure are calculated in such a way that we can set directly the settling time and the damping factor of this PLL structure. The principle of the PLL is depicted in figure 18.

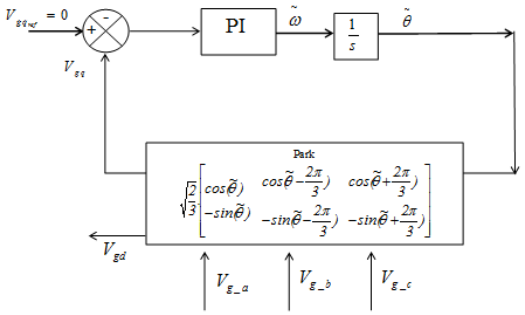

Figure 18: Block diagram of Phase locked loop

The PLL control strategy requires that the voltage be equal to zero, which allows the decoupling of the active and reactive power as presented by the equation below, [9],[10].

$$P_g = \frac{3}{2}.V_{gd}I_{gd} \qquad \text{(VI.11)}$$

$$Q_g = -\frac{3}{2}.V_{gd}I_{gq} \qquad \text{(VI.12)}$$

In addition, the relationship between the active power exchanged between the network and the DC bus is given by

$$V_{dc}.I_{dc} = \frac{3}{2}.V_{gd}.I_{gd} \qquad \text{(VI.13)}$$

7. Result of Simulation

The wind farm is based to asyncronous generator characterised by :
Nominal power : Pn=2500000 W;
Nominal voltage : Vn=690V;
Table 2 : Characteristic of asynchronous machine .

Bus capacitor C_{dc}	0.0075 F
Frequency f	50 Hz
Coefficient of friction f_r	400
Mutual inductance M	0.2037 H
Moment of inertia j	1.4 $N.m^2$
Filter inductor L_f	3.5e-4 H
Stator inductor L_s	0.0027 H
Rotor inductor L_r	0.0027H
Number of pole pairs p	2
Filter resistor R_f	3e-5 Ω
Stator resistor R_s	0.0028 Ω
Rotor resistor R_r	0.0028 Ω
Bus reference voltage V_{dcref}	1200 V

The vector control performance with the orientation of the indirect rotor flux of the asynchronous machine are evaluated using the software MATLAB / Simulink.

7.1 Wind parameter

This parameter depends on the blade number of the wind turbine. If the blade number is reduced, the rotor speed is high, and a maximum of power is extracted from the wind. In the case of multiblade wind turbines (Western Wind Turbines), the speed ratio is equal to 1; for wind turbines with a single blade, λ is about 11. The three-bladed wind turbines, as in our study, have a speed ratio of 6 to 7. The speed ratio of Savonius wind turbines is less than 1 [8]. $\mathbb{C}_p$ is the power coefficient or aerodynamic transfer efficiency that varies with the wind speed.

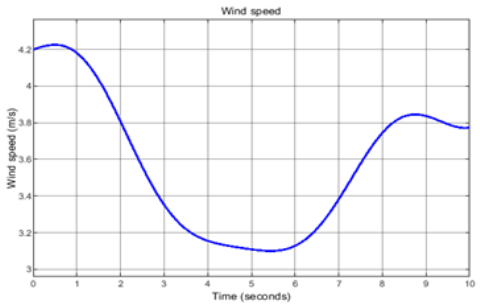

Figure 19: Wind speed evolution

This coefficient has no unit, and it depends mainly on the blade aerodynamics, the speed ratio λ, and the blade orientation angle β. Betz has determined a theoretical maximum limit of the power coefficient $\mathbb{C}_p max$= 16/27= 0.59. Taking into account losses, wind turbines never operate at this maximum limit, and the best-performing wind turbines have a $\mathbb{C}_p$ between 0.35 and 0.45. $\mathbb{C}_p$ is specific to each wind turbine, and its expression is given by the wind turbine manufacturer or using nonlinear formulas. To calculate the coefficient $\mathbb{C}_p$, different numerical approximations have been proposed in the literature.

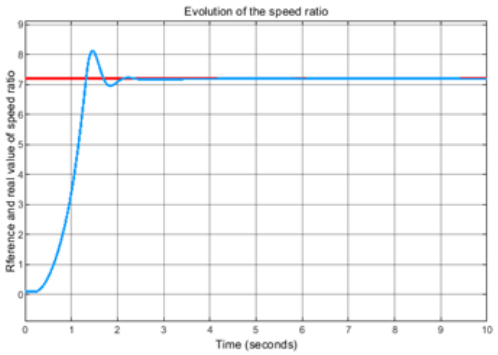

Figure 20: Speed ratio evolution

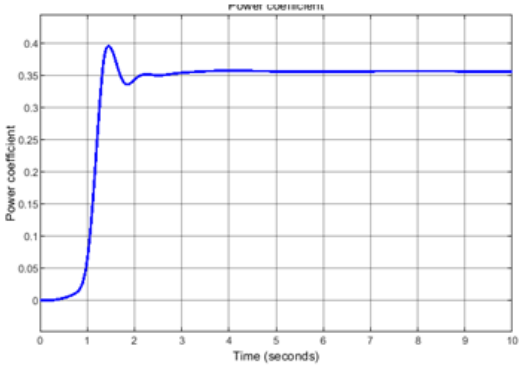

Figure 21: Power coefficient evolution

The wind speed varies between [6 m/s] and [11 m/s]. Figure 20 presents the aerodynamic power delivered by the wind turbine and it reached 3kw when the wind speed is up to 11 [m/s]. Figures 22 and 21 illustrate respectively the mechanical speed of the generator shaft and the speed of the turbine shaft. It can be noticed from during the simulation time (150 seconds), the generator operates in both hypo and hyper synchronous operating modes. The Figures 19and 20 show respectively the variation of the speed ratio λ and the variation of the power coefficient C_p and, which coincide with the optimal speed ratio and with the maximum power coefficient.

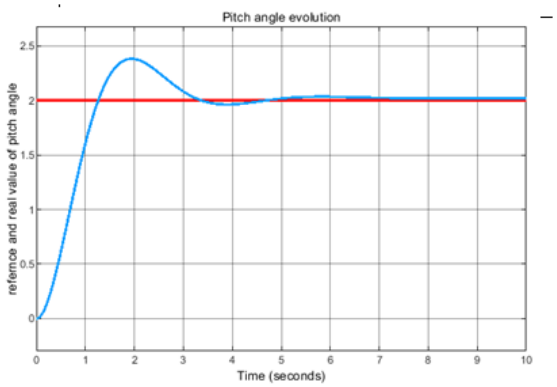

Figure 22: Pitch angle evolution

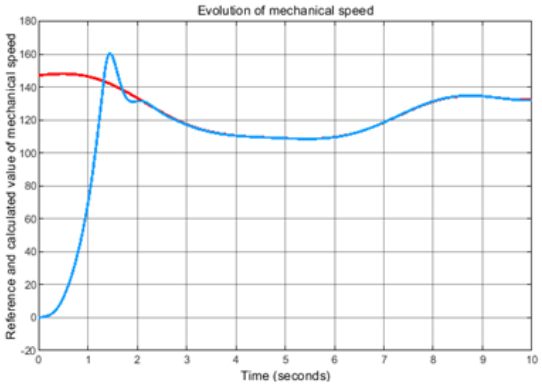

Figure 23: Mechanical speed evolution

7.2 speed variation

The system has been exposed to a real wind speed profile, in order to observe the behavior of the SCIG and its control. In Figure 24 it is possible to observe how the system evolves guided by the reference value. It is important to observe how the electromagnetic torque instantly follows the reference value. That means, it is possible to choose the operational point or follow the wind variation. Thanks to this fast control, the mechanical system, mainly the turbine, is able to quickly reach a steady state. However, the turbine speed always decreases due to the wind speed variation, despite the wind speed variation appearing filtered on the turbine by its own inertia. In Fig. 6(d), the Active Power value evolution is represented, which presents almost the same shape (just a little damped) as the wind profile. This damping is due to the multiplication of the mechanical rotation speed and the generator torque. As the generator torque almost mimics the wind shape, the damping is due to the turbine speed and its inertia, as explained before.

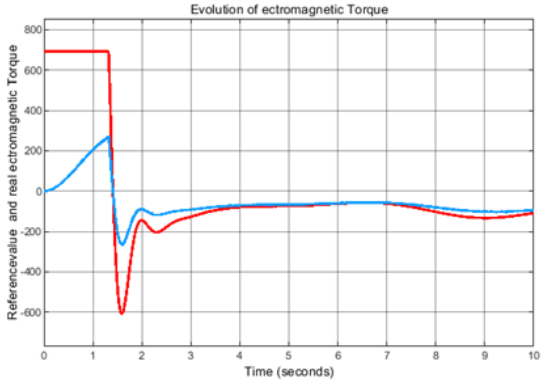

Figure 24: Electromagnetic Torque evolution

Normal PV production and average battery charge level. This scenario is characterized by a high demand for grid power to satisfy the load despite the batteries being discharged. During PV production, the system supplies to the grid and the batteries discharge.

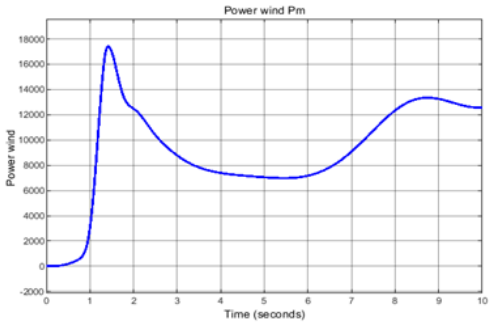

Figure 25: Power wind evolution

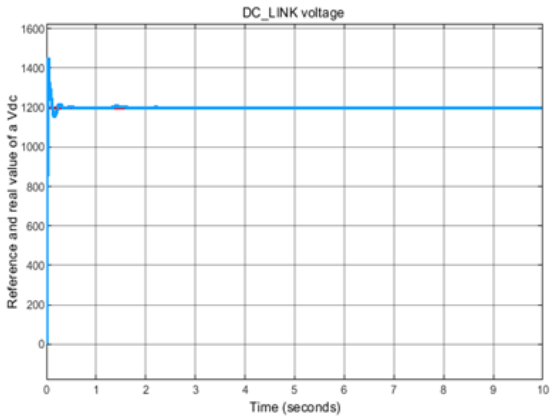

Figure 28: DC bus voltage

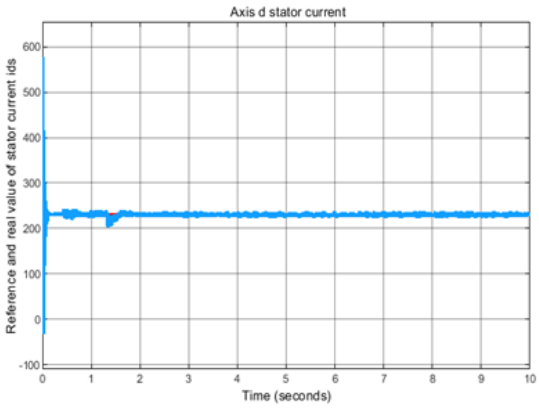

Figure 26: Axis d stator current

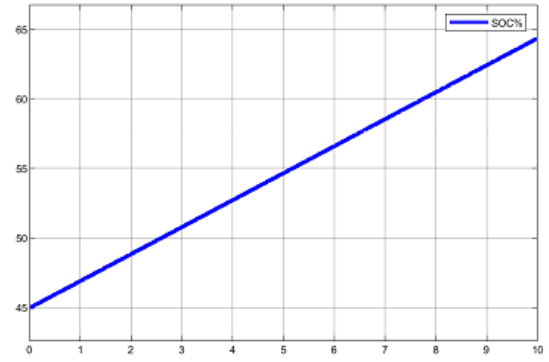

Figure 29: State of charge

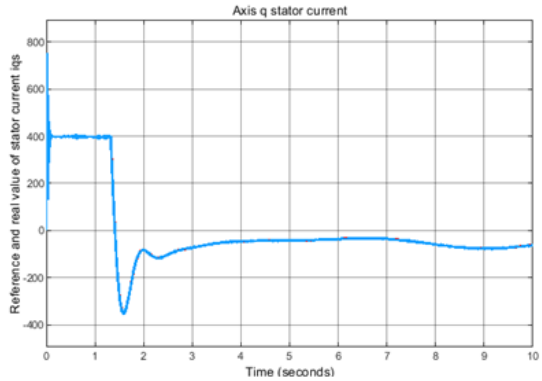

Figure 27: Axis q stator current

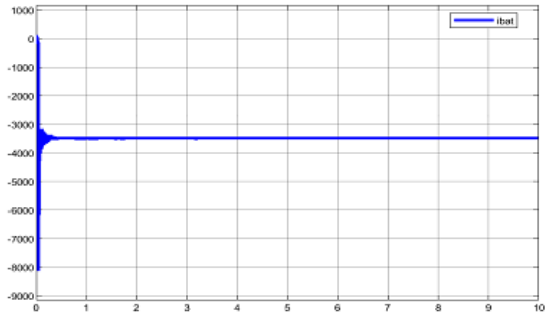

Figure 30: current of battery

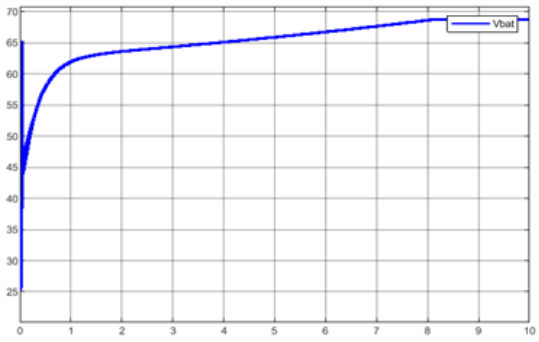

Figure 31: oltagev of battery

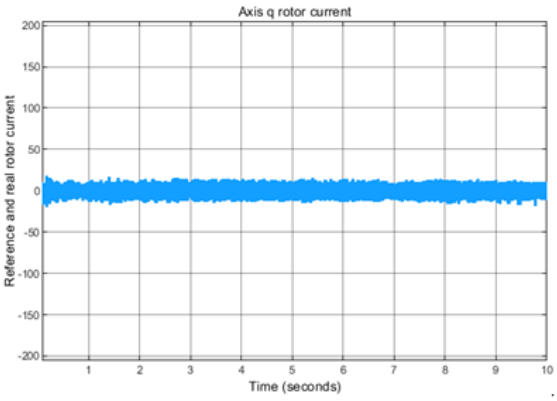

Figure 34: Axis q rotor current

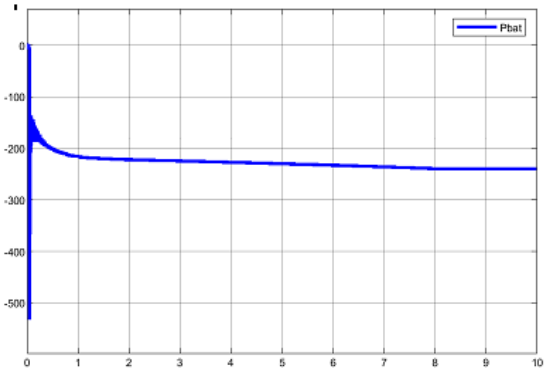

Figure 32: Power of battery

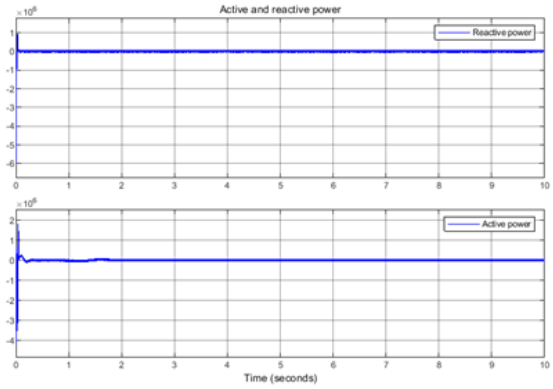

Figure 35: Reactive and active power

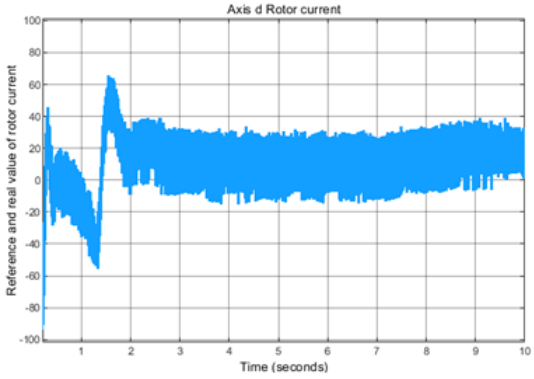

Figure 33: Axis d rotor current

8. Conclusion and future research

8.1 Conclusion

This paper presents a control technique in order to deal with a SCIG connected to the grid through a full power converter. Both stator side and grid side are taken into consideration. The control schemes used in each converter have been detailed. The vector control scheme enables the system to control the stator side converter without a flux sensor in side the machine. This fact assures fewer mechanical problems during the life time of the machine. Through this work, we have established the technique of vector control by indirect rotor flux orientation. The model flux oriented indirect control system is efficient both speed and current regulators are used. The indirect vector control proposed for the stator side converter is less dependent from machine parameters than the conventional indirect vector control, introducing to the system a faster response. . The control strategy has been satisfactorily evaluated by means of Matlab/ simulations.

8.2 Future research

By closing this chapter by proposing solutions for some problems of connection of wind system to the rid side. At the end of this work, several direct perspectives are announced and the following points are quoted by way of illustration:

* Experimental realization.
* optimizes the cost of renewable energy.
*Study of fault diagnosis and isolation algorithms.
* Study of fault-tolerant control algorithms.

References

[1] Tseligorov N. A., Ozersky A. I., Chubukin A. V., Tseligorova E. N., Development of a Robust Scalar Control System for an Induction Squirrel-cage Motor Based on a Linearized Vector Model, WSEAS Transactions on Computers, ISSN / E-ISSN: 1109-2750 / 2224-2872, Volume 21, 2022.

[2] Budhi Muliawan Suyitno, Reza Abdu Rahman, Ismail, Erlanda Augupta Pane, Increasing the Energy Density and Power Ratio of a Staggered VAWT Wind Farm by using The Rotor's Diameter as a Reference , WSEAS Transactions on Fluid Mechanics, ISSN / E-ISSN: 1790-5087 / 2224-347X, Volume 17, 2022.

[3] Salmi Hassan, Badri Abdelmajid, Zegrari Mourad, Sahel Aicha, Bagudad Abdenaceur,PSO-Backstepping Design for sharing Active and Reactive Power in grid connected DFIG based wind turbine,WSEAS Transactions on Circuits and Systems, ISSN / E-ISSN: 1109-2734 / 2224-266X, Volume 20, 2021.

[4] B. Wu, Power Conversion and Control of Wind Energy Systems, August 2011, WileyIEEE Press, ISBN: 978-0-470-59365-3.

[5] Essamudin Ali Ebrahim, Abuelmaaty M. Ali, Performance and Tracking Control of Three-Phase Induction-Motor Drive Fed from a DC-Modified Nanogrid,WSEAS Transactions on Power Systems, ISSN / E-ISSN: 1790-5060 / 2224-350X, Volume 16, 2021.

[6] A. LOKRITI, Y. Z. (10 au 12 mai 2010). COMPARAISON DES PERFORMANCES DES REGULATEURS PI ET IP APPLIQUES POUR LA COMMANDE VECTORIELLE A FLUX ROTORIQUE ORIENTE D'UNE MACHINE ASYNCHRONE. Evaluation et optimisation des systèmes innovants de production de biens et de services . Hammamet - Tunisie .

[7] Eddine, C. B. (2015). Commande vectorielle indirecte d'un moteur asynchrone alimenté par un onduleur sous défaut. Algérie.

[8] Radhwane Sadouni, A. M. (2012). Indirect Rotor Field-oriented Control (IRFOC) of a Dual Star Induction Machine (DSIM) Using a Fuzzy Controlle. Acta Polytechnica Hungarica , Vol. 9, No. 4,.

[9] Tarek GALLAH, M. F. (2007). Commande vectorielle d'un moteur asynchrone par orientation de flux rotorique.

[10] Z. S. WANG*, S. L. (2009). Indirect Rotor Field Orientation Vector Control for Induction Motor Drives in the Absence of Current Sensors.

[11] ZERBO, M. (2008). IDENTIFICATION DES PARAMÈTRES ET COMMANDE VECTORIELLE ADAPTATIVE À ORIENTATION DU FLUX ROTORIQUE DE LA MACHINE ASYNCHRONE À CAGE. Québec.

[12] Report ReGrid: Basics of wind energy. Renewables Academy (RENAC) AG, Schönhauser Allee 10-11, 10119 Berlin (Germany)

[13] J.Chatelain, Machines électriques 1 , Presse Polytechniques Romandes, 1983.

[14] P.Brunet, Introduction à la commande vectorielle des machines asynchrones , LTEG Henri BRISSON Vierzon, France.

[15] N.Caliao,Dynamic modelling and control of full yratedc onverter wind turbines, Renewable Energy 36(8)(2011)2287–2297.

[16] M.Imecs, A survey of speed and flux control structures ofs quirrel-cage induction motor drives, Tech.Rep., Acta Universitatis Sapientiae Electrical and Mechanical Engineering ,2009.

[17] J.Holtz, Sensor less control of induction motor drives, Proceedings of the IEEE 90(2002)1359–1394.

[18] M. Imecs, C. Szab, J.J. Incze, Stator-field-oriented control of the variable-excited synchronous motor: numerical simulation, in: 7th International Symposium of Hungarian Researchers on Computational Intelligence, Budapest,Hungary,2006.

[19] V. Vongmanee, Emulator of wind turbine generator using dual inverter controlled squirrel-cage induction motor, in: The Eighth International Conference on Power Electronics and Drive Systems,Taipei,Taiwan,2009.

[20] R.Leidhold ,G.Garca, M.I.Valla, Field-oriented controlled induction generator with loss minimization, IEEE Transactions on Industrial Electronics49 (2002)147–156.

[21] Sperstad, I.B.; Helseth, A.; Korpas, M. Valuation of stored energy in dynamic optimal power flow of distribution systems with energy storage. In Proceedings of the 2016 International Conference on Probabilistic Methods Applied to Power Systems (PMAPS), Beijing, China, 16–20 October 2016; pp. 1–8.

[22] Yang, D.; Wen, J.; Chan, K.W.; Cai, G. Dispatching of Wind/Battery Energy Storage Hybrid Systems Using Inner Point MethodBased Model Predictive Control. Energies 2016, 9, 629. [CrossRef]

[23] Liu, W.; Liu, Y. Hierarchical model predictive control of wind farm with energy storage system for frequency regulation during black-start. Int. J. Electr. Power Energy Syst. 2020, 119, 105893. [CrossRef]